

Er₁₇Ru₆Te₃: A highly condensed metal-rich ternary telluride

Akash Mehta, John D. Corbett*

Department of Chemistry, Iowa State University, Ames, IA 50011-3020, USA

Received 10 August 2007; received in revised form 9 January 2008; accepted 19 January 2008

Available online 5 February 2008

Abstract

Er₁₇Ru₆Te₃ is obtained from high-temperature solid-state reactions in tantalum ampoules. The structure according to single-crystal X-ray diffraction is monoclinic, *C2/m* (no. 12), *Z* = 4, *a* = 40.185(8) Å, *b* = 3.9969(8) Å, *c* = 16.037(3) Å, β = 95.12(3)°, *V* = 2565.5(9) Å³. The condensed structure consists of a complex intermetallic network of intergrown sheets of edge-sharing tetrakaidecahedra (tricapped trigonal prisms, *TCTP*), and pairs of rectangular-face-sharing bicapped trigonal prisms (*BCTP*) built of erbium and centered by ruthenium. This array also contains isolated columns of *TCTP* erbium normal to these sheets that contain tellurium. Basal face sharing of all Er polyhedra along the short *b*-axis gives rise to the three-dimensional network. Synthesis and the crystal structure of the compound are discussed.

© 2008 Published by Elsevier Inc.

Keywords: Metal-rich compounds; Electron-poor phases; Tellurides; Crystal structure; Tricapped trigonal prisms; Erbium ruthenium telluride

1. Introduction

Exploration for new materials, an important step in solid-state chemistry, has led to the discovery of many compounds with diverse properties and to better understanding of structure, bonding, and what is possible in the solid state. Exploratory research in rare-earth-metal telluride chemistry has been pursued with the principal objective of expanding the boundaries for the relatively electron-poor, metal-rich systems [1]. Earlier synthetic explorations of ternary metal-rich chalcogenides, which similarly focused on the lighter chalcogenides of the early–late pairs of transition metals [2], revealed many new and novel phases, for example, Ta₈NiSe₈ [3], Hf₈ZTe₆ (*Z* = Mn–Fe) [4], Ta₁₁Z₂Se₈ (*Z* = Fe–Ni) [5], Hf₃FeTe₃ [6], Zr₆ZTe₂ (*Z* = Mn–Ni, Ru, Pt) [7], Ta₉Z₂S₆ (*Z* = Fe–Ni) [8], and Nb₆ZS₂ (*Z* = Fe–Ni) [9]. These investigations took advantage of the considerable stabilization of mixed early–late transition metal bonding that occurs in such polar intermetallics, effects that Brewer and Wengert attributed to Lewis acid–baselike donation of electrons from the late to the earlier transition metal [10]. This sort of

chemistry has been extended [11] to ternary compounds of the electron-poorer rare-earth metal (*R*) telluride systems and to the realization of many new compounds with novel compositions, structures, and properties. These include the hexagonal Fe₂P-type derivatives Dy₆ZTe₂ (*Z* = Fe–Ni) [12], Sc₆ZTe₂ (*Z* = Ru, Os, Rh, Ir) [13], Sc₆ZTe₂ (*Z* = Mn–Ni) [14] as well as the orthorhombic Sc₆ZTe₂ (*Z* = Cu, Ag, Cd) [15], Sc₆PdTe₂ [16], R₆ZTe₂ (*R* = Y; *Z* = Y, Rh, Pd, Ag; *R* = Lu; *Z* = Cu, Ag) [17]. The last group can be viewed as derivatives (through substitution of *Z* for Te) of the binary Sc₂Te-type [18] structure also known for Dy₂Te and Gd₂Te [19]. The collection of structures reflect strong heterometallic interactions between the rare-earth and late transition metals, including many 4*d* and 5*d* members in the latter role, evidently a key factor in their stabilization. (Still, it is important to remember that such ‘stabilities’ (or not) are always relative to the stability of alternate phases at that particular composition.)

Explorations of ternary transition-metal systems have been very productive. Many of the recently reported metal-rich chalcogenides have common structural motifs of tetrakaidecahedra (tricapped trigonal prisms, *TCTP*) of the earlier metal centered by a later transition metal (see [20]). With *TCTP* as fundamental building blocks, different structures can be constructed via different modes of

*Corresponding author. Fax: +1 515 294 6789.

E-mail address: jcorbett@iastate.edu (J.D. Corbett).

condensation, e.g., in the tellurides, R_6ZTe_2 ($R = \text{Gd, Er, Z = Co, Ni, Ru}$ [21]; $R = \text{Sc, Z = Ru, Rh, Ir, Os}$ [13]) versus $R_7Z_2Te_2$ ($R = \text{Er, Z = Ni}$ [22]; $R = \text{Lu, Z = Ni, Pd, Ru}$ [23]). Others contain fundamental building units of infinite, puckered chains of rare-earth metals in six rings that sandwich later transition metals, for example, $R_5Z_2Te_2$ ($R = \text{Sc, Z = Ni}$ [24]; $R = \text{Y, Z = Fe, Co, Ni}$ [25]; $R = \text{Er, Z = Co, Ni}$ [26]). Both groups can be related to the parent compound Gd_3MnI_3 [27]. Here we report $\text{Er}_{17}\text{Ru}_6\text{Te}_3$; in which waist-capped Er_6Ru trigonal prisms play a dominant structural role. The compound has the highest rare-earth-metal to tellurium ratio after Lu_8Te and Lu_7Te [28].

2. Experimental section

2.1. Syntheses

Owing to the high sensitivity of several components of the Er–Ru–Te systems toward air and moisture, all manipulations were performed inside He- or N_2 -filled glove boxes. The elements were used as received: Er metal (99.995 at% total, Ames Laboratory), Ru metal (99.95%, Ames Laboratory), Te (99.99%, Aldrich), all as chunks. The synthesis of $\text{Er}_{17}\text{Ru}_6\text{Te}_3$ began with the preparation of ErTe, for which the elements in a 1:1 molar ratio were sealed inside a silica tube under high vacuum. This was slowly heated to 450 °C, held for 2 days, heated at 750 °C for 3 days, and then radiatively cooled. The product ErTe (>95% yield) (NaCl-type structure) was single phase according to powder X-ray diffraction, and no sign of side reactions with the walls of the silica was visible. The mixed components ErTe, Er, and Ru in 7:2:2 proportions were pressed into a 5 mm pellet with a hydraulic press inside the glove box. This was arc-melted at 30 A for 30 s/side inside an Ar-filled glove box to give a shining button with a weight loss of around 2 wt%. The button wrapped in Mo foil was loaded into a 9-mm i.d. tantalum tube welded at one end, the other end of the tube was crimped shut inside the glove box, and the tube was transferred to an Ar-filled arc-welder and sealed. The tube was mounted inside a graphite-heated high vacuum furnace (Labmaster Thermal Technology Inc. 1000-2560-FP20), which was first evacuated for 1 day under high vacuum (10^{-7} Torr). The button was then sintered at 1250 °C for 2 weeks, cooled to 700 °C at 10 °C/h, and then allowed to cool radiatively. Its X-ray diffraction powder pattern showed what was subsequently found to be $\text{Er}_{17}\text{Ru}_6\text{Te}_3$ in >60% yield, with ErTe as the other major phase. After the structure and composition had been determined, a comparable reaction of a 17:6:3 Er:Ru:Te composition gave $\text{Er}_{17}\text{Ru}_6\text{Te}_3$ in >90% yield, plus a slight trace of ErTe. The powdered compound decomposes within an hour upon exposure to moist air at room temperature.

2.2. Powder X-ray diffraction

Powder diffraction patterns were recorded in the 2θ range of 4–100° over a period of 60 min with the aid of a

Huber Guinier 670 image-plate diffractometer and Cu $K\alpha_1$ radiation. Samples were first ground to a fine powder and evenly distributed between two Mylar films. These were then mounted between Al-rings in the glove box for protection against air and moisture.

2.3. Single-crystal X-ray diffraction

Thin plate-shaped black crystals were mounted inside 0.3-mm i.d. thin-walled glass capillaries in an Ar-filled glove box, and these were first closed vacuum grease and then later flame sealed outside of the box. Data collections were made with the aid of a Bruker APEX CCD-based X-ray diffractometer over a sphere of reciprocal space to $2\theta_{\text{max}} = 56.6^\circ$ with 10 s/frame exposures. The reflection intensities were integrated with SAINTPLUS 6.22 [29] subprogram, and absorption effects were corrected by means of SADABS [30]. The reflection condition $h+k = 2n$ for the monoclinic cell indicated a *C*-centered cell, the mean value of $|E^2 - 1| = 1.167$ strongly suggested centrosymmetry, and the space group $C2/m$ (no. 12) was chosen. The structure was solved by direct methods and refined on F^2 with the aid of SHELXTL 6.10 [31]. The final anisotropic refinement converged at $R1 = 0.0510$, $wR2 = 0.1401$ for $I > 2\sigma(I)$. The largest Fourier difference map residuals, 10.722 and $-4.817 \text{ e}^-/\text{\AA}^3$, located 1.16 and 1.27 Å from Te1 and Te2, respectively, resulted from inadequate absorption corrections. An alternative, transition metal–Te mixing has never been observed in such ternary rare-earth-metal compounds, and variations in lattice constants with altered synthetic compositions that would suggest a range were not observed in this system either. Some crystal and refinement parameters are summarized in Table 1 and the positional data given in Table 2 have been reduced to the standard settings with TIDY [32]. The unit cell parameters listed in Table 1, and the nearest-neighbor distances given in Table 3 have been obtained with the use of lattice dimensions from Guinier X-ray powder diffraction.

3. Results and discussion

3.1. Synthesis

Synthesis of $\text{Er}_{17}\text{Ru}_6\text{Te}_3$ was similar to that of earlier reported Er_6RuTe_2 [21]. The present compound was obtained in >90% from a suitable Er, Ru, ErTe mixture that had been arc-melted and then equilibrated for 2 weeks at 1250 °C. This compares with the evident synthesis of Er_6RuTe_2 in a 80–90% yield directly from a mixture of Er_3Ru (made by arc-melting Er and Ru) with Er_2Te_3 at 1000 °C for 10 days without further arc-melting [21]. Both processes are intended to shorten diffusion path lengths and thus to give more rapid reactions between certain combinations of the reactants. As above, prior arc-melting of the reactants has proven to be useful in the synthesis of Lu_8Te [28] (followed by 1000 °C for 2 weeks), $\text{Lu}_7\text{Z}_2\text{Te}_2$

Table 1
Crystallographic and refinement data for Er₁₇Ru₆Te₃

Formula mass (amu)	3832.6
Space group	<i>C2/m</i> (no. 12)
Unit-cell dimensions ^a (Å, deg, Å ³)	
<i>a</i>	40.185(8)
<i>b</i>	3.9969(8)
<i>c</i>	16.037(3)
β	95.12(3)
Volume	2565.5(9)
<i>Z</i>	4
<i>d</i> _{calc} (Mg/m ³)	9.923
Temperature (K)	293(2)
Crystal dimensions (mm)	0.3 × 0.1 × 0.1
Radiation	Graphite monochromated Mo <i>K</i> α, $\lambda = 0.71073$ Å
θ Range for data collection	1.02–28.30°
Index ranges	−51 < = <i>h</i> < = 51, −5 < = <i>k</i> < = 5, −21 < = <i>l</i> < = 21
Completeness for theta = 28.30°, %	94.4
Reflections collected, <i>R</i> _(int)	11181, 0.0824
Obs. indep. reflections [<i>I</i> > 2σ(<i>I</i>)]	3439
Data/restraints/parameters	3439/0/160
Absorption coeff. (Mo <i>K</i> α) (mm ^{−1})	61.620
<i>F</i> (000)	6304
Absorption correction	SADABS
Goodness-of-fit on <i>F</i> ²	1.059
<i>R</i> ₁ , <i>wR</i> ₂ [<i>I</i> > 2σ(<i>I</i>)] (all data)	0.0510, 0.1401 0.0597, 0.1451
Largest diff. peak and hole (e [−] /Å ³)	10.72, −4.82

^aFrom Guinier data obtained with Cu*K*α radiation ($\lambda = 1.54050$ Å) at 293 K.

[23] (*Z* = Ni, Pd, Ru; 1200 °C for 2 days), and Lu₁₁Te₄ [33] (1300 °C for 2 days). Nonetheless, the refractory nature of these particular *R*, *Z* metals evidently may still afford some hindrance to reaction and, as before [34], their prior reaction to form a binary intermetallic, Er₃Ru, for example, clearly seems to be helpful in reducing the time and temperatures necessary to gain good yields of single crystals.

3.2. Structure

The large ratio of metal to tellurium in this compound means a high degree of condensation is present, the Ru being characteristically centered in TCTP of Er. Fig. 1 shows about one-half (*a*/2) of a near-[010] section of the monoclinic Er₁₇Ru₆Te₃ (*C2/m*) along the short (~4.00 Å) *b*-axis. (A labeled view of the complete cell is available in Supporting data.) The relatively few Te atoms are located in isolated columns that run through the structure along *b*, but representations of their bonding to the surrounding Er are not marked. The metal atom part of the structure is made up of two types of Er-based, Ru-centered building blocks: TCTP (tetrakaidecahedra), Fig. 2a, and rectangu-

Table 2
Atomic coordinates and equivalent isotropic displacement parameters (Å² × 10³) for Er₁₇Ru₆Te₃

Atom	Wyck sym.	Site sym.	<i>x</i> ^a	<i>z</i>	<i>U</i> _(eq) ^{b,c}
Er1	4 <i>i</i>	<i>m</i>	0.7020(1)	0.1253(1)	12(1)
Er2	4 <i>i</i>	<i>m</i>	0.2695(1)	0.0716(1)	11(1)
Er3	4 <i>i</i>	<i>m</i>	0.2681(1)	0.5858(1)	14(1)
Er4	4 <i>i</i>	<i>m</i>	0.3037(1)	0.3984(1)	12(1)
Er5	4 <i>i</i>	<i>m</i>	0.1770(1)	0.2917(1)	10(1)
Er6	4 <i>i</i>	<i>m</i>	0.1311(1)	0.5971(1)	8(1)
Er7	4 <i>i</i>	<i>m</i>	0.1851(1)	0.7809(1)	12(1)
Er8	4 <i>i</i>	<i>m</i>	0.0903(1)	0.2680(1)	7(1)
Er9	2 <i>a</i>	2/ <i>m</i>	0	0	13(1)
Er10	2 <i>c</i>	2/ <i>m</i>	0	0.5000	14(1)
Er11	4 <i>i</i>	<i>m</i>	0.3563(1)	0.0781(1)	13(1)
Er12	4 <i>i</i>	<i>m</i>	0.4720(1)	0.1627(1)	11(1)
Er13	4 <i>i</i>	<i>m</i>	0.4411(1)	0.3888(1)	12(1)
Er14	4 <i>i</i>	<i>m</i>	0.0935(1)	0.7716(1)	7(1)
Er15	4 <i>i</i>	<i>m</i>	0.5260(1)	0.3347(1)	11(1)
Er16	4 <i>i</i>	<i>m</i>	0.1337(1)	0.0963(1)	7(1)
Er17	4 <i>i</i>	<i>m</i>	0.3618(1)	0.5778(1)	13(1)
Er18	4 <i>i</i>	<i>m</i>	0.5588(1)	0.1093(1)	12(1)
Ru1	4 <i>i</i>	<i>m</i>	0.8085(1)	0.0070(1)	7(1)
Ru2	4 <i>i</i>	<i>m</i>	0.1884(1)	0.4786(1)	8(1)
Ru3	4 <i>i</i>	<i>m</i>	0.3620(1)	0.2770(1)	7(1)
Ru4	4 <i>i</i>	<i>m</i>	0.0233(1)	0.1897(1)	6(1)
Ru5	4 <i>i</i>	<i>m</i>	0.0252(1)	0.6928(1)	6(1)
Ru6	4 <i>i</i>	<i>m</i>	0.6347(1)	0.2207(1)	7(1)
Te1	4 <i>i</i>	<i>m</i>	0.2499(1)	0.2529(1)	11(1)
Te2	4 <i>i</i>	<i>m</i>	0.0740(1)	0.4539(1)	4(1)
Te3	4 <i>i</i>	<i>m</i>	0.9240(1)	0.0448(1)	5(1)

^a*y* = 0 for all atoms.

^b*U*_(eq) is defined as one-third of the trace of the orthogonalized *U*^{*ij*} tensor.

^cAnisotropic displacement parameters appear in the cif file—see Supplementary data.

lar-face-sharing bicapped trigonal prisms (*BCTP*)₂, Fig. 2b. Both share trigonal basal faces along the *b*-axis to generate the infinite three-dimensional structure. The common bifunctional character of the Er atoms in many edge-sharing TCTP—prismatic in one cluster and face capping in the next—gives rise to a corrugation of the prisms pairs in the *a*–*b* plane, as can be seen in Fig. 1b.

The Er–Er, Er–Ru, and Er–Te bond distances (Table 3) in Er₁₇Ru₆Te₃ are comparable to those observed in other ternary tellurides of late rare-earth and heavy transition metals, for example, in *R*₆*Z*Te₂ [17,21] (*R* = Y, Gd, Er; *Z* = Ru, Rh, Pd) and *R*₇*Z*₂Te₂ [23] (*R* = Lu; *Z* = Pd, Ru). The Er TCTP surroundings about most Ru generally consist of six close and three ~0.3 Å more distant Er neighbors, corresponding to the trigonal prismatic and the face-capping dispositions, respectively. However, a few of the secondary Er–Ru values are as much as 0.5–0.6 Å longer because of distortions necessary in fitting the TCTP and BCTP into this rather complex array. Of course, Ru in the BCTP dimers is only eight-bonded to Er, and this leads to shorter face-capping Ru–Er interactions on the back side. Interestingly, the Er–Te distance distribution is nearly reversed from that of Er–Ru, for the following reasons:

Table 3
Bond distances (Å) for Er₁₇Ru₆Te₃

Atom 1	Atom 2	×	Distance	Atom 1	Atom 2	×	Distance	Atom 1	Atom 2	×	Distance	
Er1	Ru1	2	2.918(1)	Er9	Ru4	2	3.102(2)	Er18	Er8	2	3.601(1)	
	Ru6	1	3.224(3)		Te3	2	3.200(1)		Er3	1	3.775(1)	
	Te1	2	3.344(1)		Er18	4	3.450(1)		Ru4	2	2.833(1)	
	Er16	2	3.394(1)		Er12	4	3.548(1)		Te3	2	3.299(1)	
	Er2	1	3.455(1)		Er10	Te2	2		3.128(1)	Er8	2	3.392(1)
	Er2	2	3.537(1)			Ru5	2		3.167(2)	Ru6	1	3.396(3)
Er2	Er5	2	3.550(1)	Er15	4	3.467(1)	Er9	2	3.450(1)			
	Ru1	2	2.796(1)	Er11	Ru1	2	2.931(1)	Er16	2	3.635(1)		
	Te1	1	3.078(2)		Ru3	1	3.177(2)	Er12	1	3.663(2)		
	Ru1	1	3.273(3)		Te3	2	3.453(1)	Er15	1	3.958(1)		
	Er2	2	3.329(2)		Er2	1	3.482(1)	Ru1	Er2	2	2.796(1)	
	Er1	1	3.455(2)		Er16	2	3.490(1)	Er1	2	2.918(1)		
Er11	1	3.482(2)	Er7		2	3.542(1)	Er11	2	2.931(2)			
Er3	Er7	2	3.487(1)	Er14	2	3.604(1)	Er16	1	2.970(2)			
	Er1	2	3.537(1)	Er12	Er1	1	3.844(1)	Er2	1	3.273(3)		
	Ru2	2	2.902(1)		Ru4	2	2.874(1)	Er7	1	3.389(3)		
	Te1	2	3.399(1)		Ru5	2	3.055(1)	Ru2	Er4	2	2.807(1)	
	Er4	2	3.442(2)		Tu3	2	3.263(1)	Er3	2	2.902(1)		
	Er5	1	3.457(1)		Er15	1	3.352(1)	Er17	2	2.924(1)		
Ru2	1	3.497(3)	Er14		2	3.542(1)	Er5	1	2.991(1)			
Er4	Er4	2	3.540(1)	Er9	2	3.548(1)	Er6	1	3.115(1)			
	Er3	2	3.601(2)	Er18	1	3.663(2)	Er3	1	3.497(1)			
	Er17	1	3.775(1)	Er13	1	3.937(1)	Ru3	Er14	2	2.835(1)		
	Ru2	3	2.807(1)	Er13	Ru5	2	2.803(1)	Er6	2	2.837(1)		
	Te1	1	3.036(2)	Er13	Te2	2	3.317(1)	Er7	2	2.849(1)		
	Ru3	1	3.176(3)		Er14	2	3.451(1)	Er4	1	3.176(1)		
Er6	2	3.290(1)	Er10		2	3.467(1)	Er11	1	3.177(1)			
Er3	2	3.540(1)	Ru3		1	3.508(3)	Er13	1	3.508(1)			
Er17	1	3.539(2)	Er6		2	3.547(1)	Ru4	Er18	2	2.833(1)		
Er7	2	3.562(1)	Er15		1	3.592(1)	Er8	1	2.868(1)			
Er5	Ru6	2	2.798(1)	Er12	1	3.937(1)	Er12	2	2.874(1)			
	Ru2	1	2.991(2)	Er14	Ru3	2	2.835(1)	Er15	2	3.061(1)		
	Te1	1	3.051(2)		Ru5	1	2.918(2)	Er9	1	3.102(1)		
	Er17	2	3.373(1)		Te3	1	3.088(1)	Ru5	Er13	2	2.803(1)	
	Er16	1	3.444(1)		Er6	1	3.296(2)	Er15	2	2.873(1)		
	Er3	2	3.457(1)		Er13	2	3.451(1)	Er14	1	2.918(1)		
Er8	1	3.470(1)	Er12		2	3.542(1)	Er12	2	3.055(1)			
Er6	Er1	2	3.550(1)	Er11	2	3.604(1)	Er10	1	3.167(1)			
	Ru3	2	2.837(1)	Er7	1	3.664(2)	Ru6	Er5	2	2.798(1)		
	Te2	1	3.098(2)	Er15	Er5	2	2.873(1)	Er16	2	2.822(1)		
	Ru2	1	3.115(2)		Ru4	2	3.061(1)	Er8	2	2.828(1)		
	Er4	2	3.290(1)		Te2	2	3.274(1)	Er1	1	3.224(1)		
	Er14	1	3.296(1)		Er12	1	3.352(2)	Er17	1	3.221(2)		
Er17	2	3.477(1)	Er8		2	3.509(1)	Er18	1	3.396(1)			
Er7	1	3.500(2)	Er10		2	3.550(1)	Te1	Er4	1	3.036(1)		
Er7	Er13	2	3.547(1)	Er13	1	3.592(1)	Er5	1	3.051(1)			
	Ru3	2	2.849(1)	Er18	1	3.958(1)	Er2	1	3.078(1)			
	Te1	2	3.372(1)	Er16	Er8	2	2.822(1)	Er1	2	3.344(1)		
	Ru1	1	3.389(3)		Ru6	2	2.822(1)	Er7	2	3.372(1)		
	Er2	2	3.487(1)		Ru1	1	2.970(2)	Er3	2	3.399(1)		
	Er6	1	3.500(2)		Te3	1	3.091(2)	Te2	Er6	1	3.098(1)	
Er11	2	3.542(1)	Er8		1	3.389(1)	Er8	1	3.107(1)			
Er4	2	3.562(1)	Er1		2	3.394(1)	Er10	1	3.128(1)			
Er8	Er14	1	3.664(2)	Er5	1	3.444(1)	Er15	2	3.274(1)			
	Ru6	2	2.828(1)	Er11	2	3.490(1)	Er13	2	3.317(1)			
	Ru4	1	2.868(2)	Er18	2	3.635(1)	Er17	2	3.339(1)			
	Te2	1	3.107(1)	Er17	Ru2	2	2.924(1)	Te3	Er14	1	3.088(2)	
	Er16	1	3.389(1)		Ru6	1	3.221(2)	Er16	1	3.091(2)		
	Er18	2	3.392(1)		Te2	2	3.339(1)	Er9	1	3.200(1)		
Er5	1	3.468(2)	Er5		2	3.373(1)	Er12	2	3.263(1)			
Er15	2	3.509(1)	Er6		2	3.477(1)	Er18	2	3.299(1)			
Er17	2	3.601(1)	Er4		1	3.539(1)	Er11	2	3.453(1)			

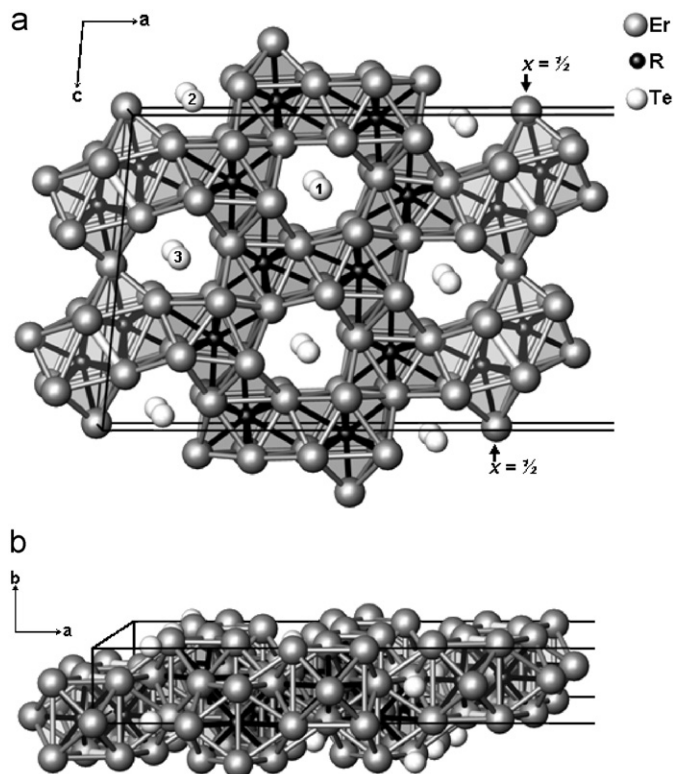


Fig. 1. The crystal structure of $\text{Er}_{17}\text{Ru}_6\text{Te}_3$: (a) slightly off $[010]$ section of one-half of the monoclinic cell. Ru (black) centers the Er-based *TCTP* (dark gray), and rectangular-face-sharing *BCTP* (light gray), with Er–Er (gray) and Er–Ru (black) bonds marked. Bonding to Te (white) within the *TCTP* is not shown for clarity. (b) Corrugation in a section of the 2D layer viewed approximately along $[101]$. The partial boundaries of the unit cell are shown in black.

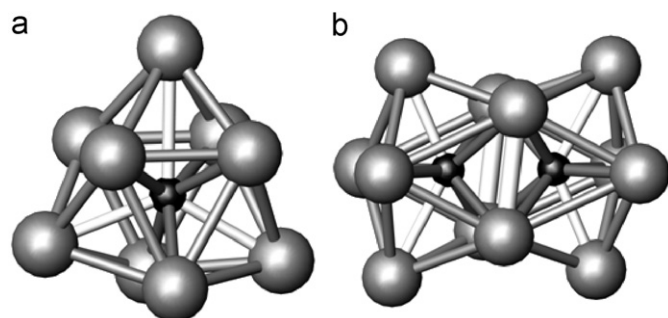


Fig. 2. Main building blocks in $\text{Er}_{17}\text{Ru}_6\text{Te}_3$. (a) RuEr_9 : a *TCTP* with dark gray Ru–Er bonds in trigonal prism and white bonds to face-capping atoms. (b) $\text{Ru}_2\text{Er}_{12}$: a pair of rectangular-face-sharing bicapped trigonal prisms (*BCTP*)₂ in which the shared face is marked by thicker white Er–Er bonds.

The prism heights are all the same, $b = 4.00 \text{ \AA}$, and the structure adapts to the somewhat larger Te by lengthening the basal edges and thereby $d(\text{Te}-\text{Er}_{\text{prism}})$ by about 0.4 \AA to yield a range of 3.2 to 3.4 \AA (Table 3). This in effect decreases the face capping $d(\text{Te}-\text{Er}_{\text{f.c.}})$ to around 3.1 \AA . The bonding of Ru within the *TCTP* of Er involves very different types of interactions than for Te within Er *TCTP*.

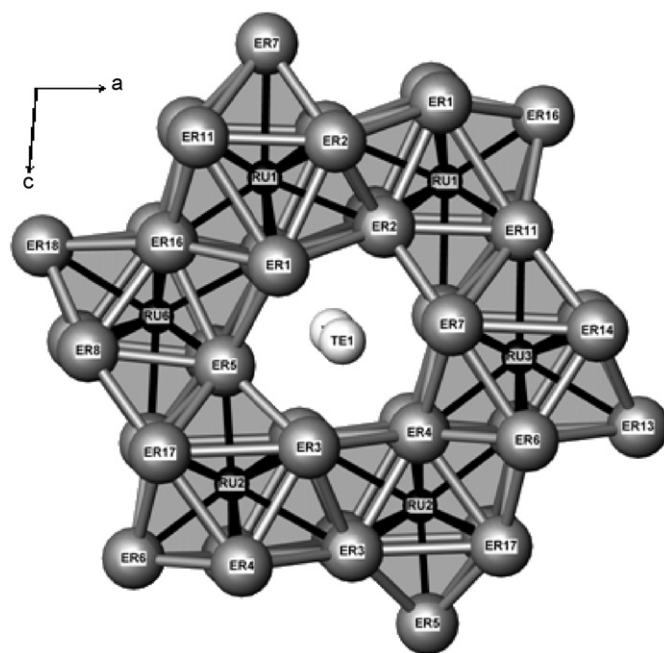


Fig. 3. Puckered hexagonal channel about Te1 defined by the face-sharing Ru-*TCTP*; $[010]$ view.

Most Er–Er separations in $\text{Er}_{17}\text{Ru}_6\text{Te}_3$ appear relatively uniform, over a range of ~ 3.3 – 3.6 \AA . All Er have a single Te neighbor in an adjoining tunnel except for the unusual bridging Er9 and Er10 (below). The shortest $d(\text{Er}-\text{Er})$ are for Er4–Er6 and Er6–Er14, $\sim 3.3 \text{ \AA}$, whereas even longer $d(\text{Er}-\text{Er})$ values occur for Er pairs 7–14, 3–17, and 1–11, 3.66 , 3.78 , and 3.84 \AA . It is noteworthy that all of these shorter and longer separations occur in the seam between the Te1 and the Te2, Te3 regions at the outside edges of the darker area in Fig. 1 (and Fig. 4 below) in which much of the strain must be located.

The Te1 atoms are, as for Ru, surrounded by nine-membered *TCTPs* of Er, Fig. 3. These channels are defined by distorted edge-sharing Ru-centered *TCTPs*, which mean that the hexagonal edges seen in projection are puckered, and the channels exhibit different bonding environments along $[001]$ and $[100]$. The *TCTP* rings about each Te1 are shared along $[001]$, the dark area in Fig. 1a, with a stacking angle of $\beta = 95.12^\circ$.

Fig. 4 illustrates how the remaining Te2 and Te3 in $\text{Er}_{17}\text{Ru}_6\text{Te}_3$ are accommodated within pairs of adjacent *TCTP* hexagonal channels that extend along $[001]$. This area is centered around the 200 planes ($x = 0, \frac{1}{2}$) and thus appears split at the two outside edges of the area shown in Fig. 1a, a separate representation being used to retain details in the figures. The polyhedra about the two Te are seen to be interconnected along $[100]$ via tilted pairs of rectangular-face-sharing (*BCTP*)₂ units (${}^1_{\infty}[\text{Ru}_2\text{Er}_{12}]$) (Fig. 2b). These (*BCTP*)₂ units are further interconnected along $[001]$ by two outer (face capping) Er9, Er10 atoms which lie on special positions and are inter-related by $z = \frac{1}{2}$. The different arrangements of two different construction polyhedra, viz., *TCTP* and (*BCTP*)₂, give rise to three

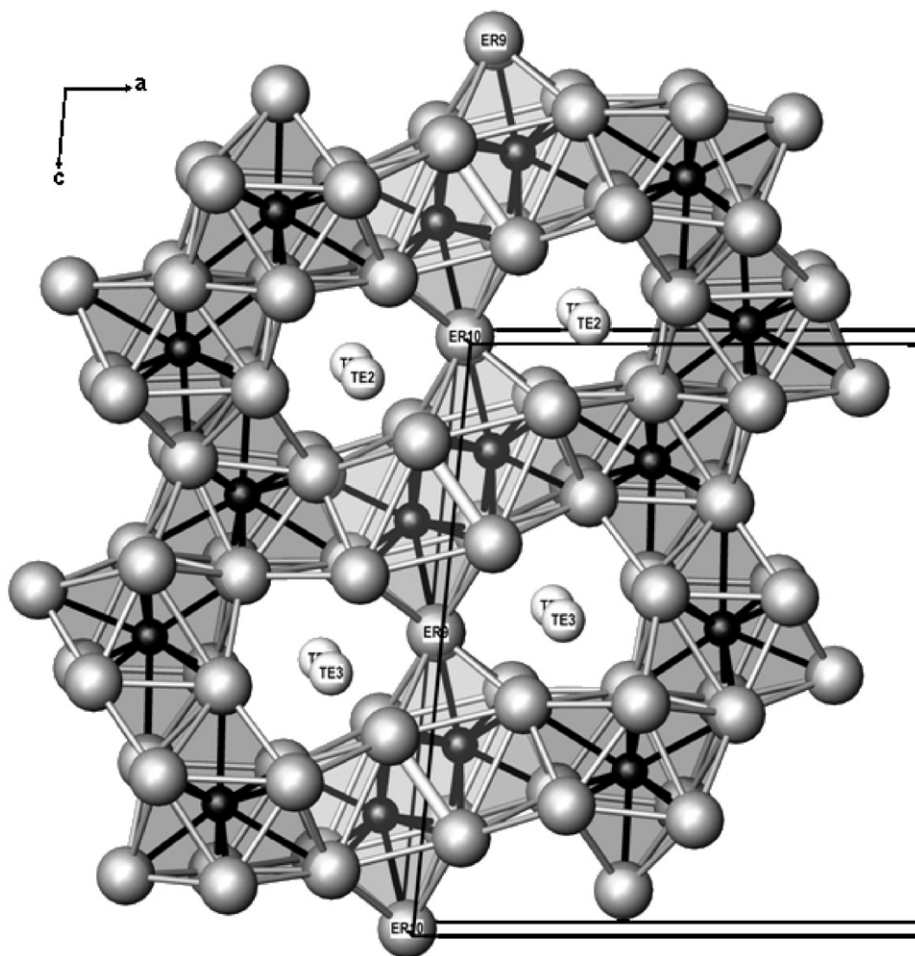


Fig. 4. Pairs of trigonal prismatic Er channels that define Te2 and Te3 sites. The framework is made up of rectangular-face-shared *BCTP* (light-gray polyhedra) along [010] and corner-shared Er9 and Er10 along [001]. The Te2, Te3, and Er9, Er10 pairs are each related by $z \sim \frac{1}{2}$ (see text).

distorted hexagonal channel types for the anions, Te1 in Fig. 3, and paired channels between $(BCTP)_2$ for Te2 and Te3 (Fig. 4). Nearly a regular difference, 0, 0, $\sim \frac{1}{2}$, can be found between Te2 versus Te3 coordinates (Table 2) on consideration of equivalent positions, but this is only an isolated pseudo-symmetry in space group $C2/m$. The roles of the formal Te^{-2} in all of this family of compounds are principally those of large spacers between or within polymetal cationic clusters, in contrast to the much more structurally specific roles the anions play in metal-rich halides of the same elements [11].

The occurrence of both *TCTP* and rectangular-face-sharing $(BCTP)_2$ polyhedra appears to be unique to this structure. Some rare-earth metal–transition-metal tellurides are fully constituted of only *TCTP* rare-earth metals, for example, R_6ZTe_2 ($R = Sc$; $Z = Ru, Rh, Ir, Os$ [13]; $R = Sc$; $Z = Mn, Fe, Co, Ni, Cu, Ag, Cd$ [14,15]; $R_7Z_2Te_2$ ($R = Er$; $Z = Ni, Ir$ [22,35]; $R = Lu$; $Z = Ni, Pd, Ru$ [23]; $R = Y, Z = Os, Pt$ [35].) We are not aware of any other example containing $(BCTP)_2$. The compound $Er_{17}Ru_6Te_3$ is the fourth in a series of the rare-earth metal richest tellurides after Lu_8Te , Lu_7Te [28], and the newly discovered and even more condensed, $Er_{21}Ir_8Te_4$ [36], but the ternary

phases are second and third in terms of fractional metal contents.

4. Conclusions

The highly condensed, metal-rich ternary telluride $Er_{17}Ru_6Te_3$ has been synthesized by high-temperature annealing after arc-melting. The complex crystal structure of $Er_{17}Ru_6Te_3$ can be visualized in terms of condensed Ru-centered *TCTP* and face-sharing $(BCTP)_2$ of Er in an array that also generates three types of parallel channels of *TCTP* of Er that bind Te. The metal-richest portions of ternary rare-earth metal–transition-metal–tellurium systems have evidently not been well investigated, and more-detailed explorations will definitely uncover more novel compounds.

Acknowledgment

This research was supported by the National Science Foundation, Solid State Chemistry, via Grant DMR-0444657 and was performed in the US Department of Energy's Ames Laboratory at Iowa State University.

Appendix A. Supplementary data

The CIF file can be obtained from the Fachinformationszentrum Karlsruhe, 76344 Eggenstein-Leopoldshafen, Germany (fax: +49 7247 808 666; e-mail address: crysdata@fiz.karlsruhe.de) on quoting the depository number CSD-391431. A [010] projection of the complete unit cell of $\text{Er}_{17}\text{Ru}_6\text{Te}_3$ with the atoms labeled is available on the Web version of this publication.

Supplementary data associated with this article can be found in the online version at [doi:10.1016/j.jssc.2007.11.020](https://doi.org/10.1016/j.jssc.2007.11.020).

References

- [1] J.D. Corbett, *Inorganic Chemistry in Focus II*, Wiley-VCH Verlag GmbH & Co., Weinheim, Germany, 2005, p. 121.
- [2] T. Hughbanks, *J. Alloys Compd.* 229 (1995) 40.
- [3] M. Conrad, B. Harbrecht, *J. Alloys Compd.* 197 (1993) 57.
- [4] R.L. Abdon, T. Hughbanks, *Chem. Mater.* 6 (1994) 424.
- [5] B. Harbrecht, *J. Less-Common Met.* 141 (1988) 59.
- [6] R. L. Abdon, T. Hughbanks, *J. Am. Chem. Soc.* 117 (1995) 10035.
- [7] C. Wang, T. Hughbanks, *Inorg. Chem.* 35 (1996) 6987.
- [8] B. Harbrecht, H.F. Franzen, *J. Less-Common Met.* 113 (1985) 349.
- [9] B. Harbrecht, *Z. Kristallogr.* 182 (1988) 118.
- [10] L. Brewer, P.R. Wengert, *Metallurg. Trans.* 4 (1973) 83.
- [11] J.D. Corbett, *J. Alloys Compd.* 418 (2006) 1.
- [12] N. Bestoui, P.S. Herle, J.D. Corbett, *J. Solid State Chem.* 155 (2000) 9.
- [13] L. Chen, J.D. Corbett, *Inorg. Chem.* 43 (2004) 436.
- [14] P.A. Maggard, J.D. Corbett, *Inorg. Chem.* 39 (2000) 4143.
- [15] L. Chen, J.D. Corbett, *Inorg. Chem.* 41 (2002) 2146.
- [16] P.A. Maggard, J.D. Corbett, *J. Am. Chem. Soc.* 122 (2000) 10740.
- [17] L.M. Castro-Castro, L. Chen, J.D. Corbett, *J. Solid State Chem.* 180 (2007) 3172.
- [18] P.A. Maggard, J.D. Corbett, *Angew. Chem. Int. Ed. Engl.* 18 (1997) 11974.
- [19] P.S. Herle, J.D. Corbett, *Inorg. Chem.* 40 (2001) 1858.
- [20] B.G. Hyde, S. Andersson, *Augmented trigonal prismatic constructions*, Inorganic Crystal Structures, Wiley-Interscience Publishers, New York, 1989, p. 80.
- [21] F. Meng, C. Magliocchi, T. Hughbanks, *J. Alloys Compd.* 358 (2003) 98.
- [22] F. Meng, T. Hughbanks, *Inorg. Chem.* 40 (2001) 2482.
- [23] L. Chen, J.D. Corbett, *Inorg. Chem.* 43 (2004) 3371.
- [24] P.A. Maggard, J.D. Corbett, *Inorg. Chem.* 38 (1999) 1945.
- [25] P.A. Maggard, J.D. Corbett, *Inorg. Chem.* 43 (2004) 2556.
- [26] C. Magliocchi, F. Meng, T. Hughbanks, *J. Solid State Chem.* 177 (2004) 3896.
- [27] M. Ebihara, J.D. Martin, J.D. Corbett, *Inorg. Chem.* 33 (1994) 2078.
- [28] L. Chen, J.D. Corbett, *J. Am. Chem. Soc.* 125 (2003) 7794.
- [29] SAINTPLUS 6.22; Bruker AXS, Inc., Madison, WI, 2000.
- [30] R.H. Blessing, *Acta Crystallogr. A* 51 (1995) 33.
- [31] SHELXTL 6.10; Bruker AXS, Inc., Madison, WI, 2000.
- [32] L. M. Gelato, E.J. Parthé, *Appl. Crystallogr.* 20 (1987) 139.
- [33] L. Chen, S.-Q. Xia, J.D. Corbett, *Inorg. Chem.* 44 (2005) 3057.
- [34] T. Hughbanks, J.D. Corbett, *Inorg. Chem.* 28 (1989) 631.
- [35] L.M. Castro-Castro, A. Mehta, J.D. Corbett, unpublished results.
- [36] A. Mehta, J.D. Corbett, unpublished results.